Water effect in the synthesis of nanostructured thin films of HfO_2 deposited by the ultrasonic spray pyrolysis technique

R. Vázquez-Arreguín[a], A. González-Cisneros[a], M. García-Rocha[b],
A.G. Juarez-Gracia[c], L. Mariscal-Becerra[d], and A. A. Duran-Ledezma[a,*]

[a]*Instituto Politécnico Nacional, Escuela Superior de Cómputo,*
Av. Juan de Dios Bátiz esq. Av. Miguel Othón de Mendizábal, Lindavista, Gustavo A. Madero, México, CDMX, 07738.
[*]*e-mail: aduranl@ipn.mx*
[b]*Departamento de Física, Centro de Investigación y de Estudios Avanzados del IPN.*
Av. Instituto Politécnico Nacional 2508, San Pedro Zacatenco, Gustavo A. Madero, México CDMX. 07360.
[c]*Instituto Politécnico Nacional, Centro de Investigación en Ciencia Aplicada y Tecnología Avanzada,*
Unidad Legaria, Calzada Legaria 694, Irrigación, Miguel Hidalgo, México, CDMX, 11500.
[d]*Facultad de Ciencias, Universidad Nacional Autónoma de México,*
Circuito Exterior S/N, Ciudad Universitaria, Coyoacán, México CDMX 04510.

Received 28 December 2020; accepted 17 February 2021

HfO_2 thin films are proposed as a high-k dielectric gate, especially for the fabrication of ultra-large-scale integration systems. The effect of adding deionized water during the synthesis of HfO_2 thin films on its structural and dielectric properties is reported. The study of nanostructured HfO_2 thin films deposited on crystalline silicon wafers is made by applying the ultrasonic spray pyrolysis (USP) technique. For the synthesis of hafnium oxide thin films, hafnium acetylacetonate was dissolved in dimethylformamide as a hafnium source material. The substrate temperature was varied from 400°C and up to 550°C in increments of 50°C and adding deionized water during the process, favoring films with well-defined monoclinic structures. The thin films presented a nanostructured morphology and a rugosity with a minimum value of 0.45 nm. Refractive index values between 1.87 and 2.02 were obtained with an average thickness of $\sim$ 21 nm. The carbon and O-H bonds decrease considerably, adding deionized water during the deposit. The electrical characterization revealed that the films deposited with deionized water have a high dielectric constant with a maximum value of 14.4, demonstrating that this addition during deposition allows thinner films with good dielectric properties.

Keywords: Nanostructured thin films; USP process; metal-organic source; crystal structures; high-K dielectrics.

PACS: 31.15.es; 68.37.Ps; 68.37.-d; 77.55.+f

DOI: https://doi.org/10.31349/RevMexFis.67.051002

1. Introduction

Continuous technological development has triggered the search for new materials that comply with specific properties for avant-garde devices and new manufacturing techniques. In the microelectronics industry, the Ultra Large-Scale Integration (ULSI) as well as the current generations of CMOS and MOSFET devices, among others, tend to require thin insulating layers of around 30 Å. Silicon dioxide (SiO_2) has been used with great success. However, for new devices, silicon dioxide films with thicknesses of $\sim$ 30 Å, present tunneling through the potential barrier and impurities diffusion. As a result, other types of materials have been investigated to replace SiO_2 [1].

In recent years, much research has been conducted on HfO_2 and related compounds thanks to their excellent physicochemical properties, high refractive index, and bandgap energy of 5.68 eV [2-3]. Its transparency extends over a wide spectral range, from ultraviolet to medium infrared [4-6]. Consequently, this material is widely utilized for optical applications as a protective layer due to its thermal stability and hardness, and it is also used as a gas sensor [7-11]. HfO_2 films are susceptible to doping with different rare earths, emitting at different colors depending on the dopant when excited with UV light. Crystallinity allows the incorporation of this type of ions [12]. The most common precursors used to synthesize HfO_2 are chlorides and metal-organics. In particular, hafnium acetylacetonate ($Hf(acac)_4$) is used due to its low melting temperature ($\approx$ 200°C), as well as its ease of dissolution in N, N-Dimethylformamide (N,N-DMF). It is a solvent with a high dissolution capacity with acetylacetonates. This solvent has successfully been used to synthesize other materials, such as aluminum and zirconium oxide [13,14]. Due to its high dielectric constant as an insulator, HfO_2 has received considerable attention in the field of microelectronics as an alternative material to silicon oxide in the next-generation MOS devices [15-16].

Many techniques have been applied in the synthesis of hafnium oxide films [17-24]. Ultrasonic spray pyrolysis has proven to be an efficient, versatile, and low cost technique for depositing thin films that can be scaled at an industrial level since it does not require a vacuum equipment operation, making the depositing processes more expensive [25-27].

The present article shows an alternative method of depositing HfO_2 thin films by adding deionized water by ul-

trasonic spray pyrolysis. HfO_2 films were also synthesized without water spray during deposition to evaluate the method, keeping the other deposition parameters constant. The characterization was carried out utilizing XRD to determine the crystalline structure formed under various growth conditions. Refractive index and thin film thickness were determined through ellipsometry. AFM shows the HfO_2 thin film surface morphology and rugosity values. With SEM, the morphology of the deposits was shown. IR measurements allowed to determine the types of existing ligands and establish water effect on the growth of HfO_2 films. Finally, the electrical characterization was done by C-V measurements, from which the dielectric constant for the films was acquired. Our results show that deposit of HfO_2 thin films by ultrasonic spray pyrolysis, adding deionized water, can be successfully used, allowing to obtain adequate dielectric values and low roughness values, making HfO_2 a right substitute candidate for SiO_2 in the fabrication of MOS structures.

2. Experimental procedure

2.1. Experimental setup

Figure 1 presents the experimental setup consisting of a compressed air tank, used as the carrier gas, a regulator at the entrance, and a flow meter. Two ultrasonic generators operate at 780 kHz, the first container restrains the Hafnium (Hf) salt dissolved in N-dimethylformamide (N,N-DMF), and the second one contains deionized water, both connected to a pair of glass nozzles joined to plastic hoses that allow directing the generated aerosol to the surface of the substrate. The separation between nozzle and substrate is 5 mm. The substrates are placed in the molten tin bath. The temperature of the system increases linearly using a controller. A thermocouple allows instant monitoring of the temperature of the tin bath. The system is enclosed in an acrylic chamber connected to a gas extraction system.

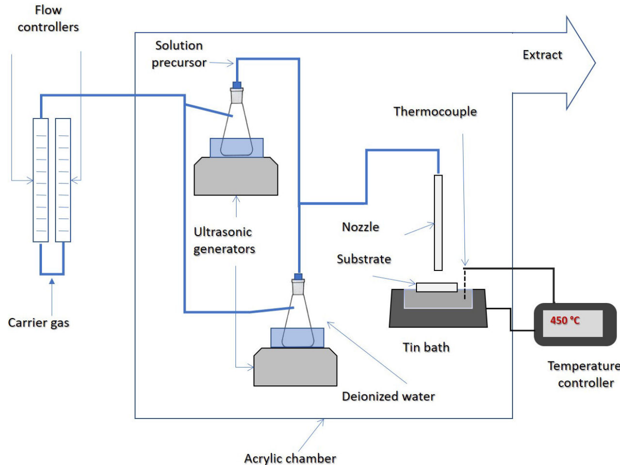

FIGURE 1. Experimental setup of ultrasonic spray pyrolysis synthesis.

2.2. Materials and synthesis of HfO_2 thin films

Hafnium oxide, HfO_2, films were synthesized by ultrasonic spray pyrolysis. Two types of substrates were employed, n-type Si (111) and Si (100), high and low resistivity, respectively, both for electrical and structural characterization.

Hafnium acetylacetonate (Hf(acac)$_4$, Alfa Aesar, 97%) and N,N-DMF were used as HfO_2 precursors at a 0.035 molarity. We followed two synthesis paths. Hf(acac)$_4$ and N,N-DMF were mixed in an ultrasonic nebulizer in the first path. Two ultrasonic nebulizers were applied; the first contains Hf(acac)$_4$ and N,N-DMF, while deionized water (18 MΩcm^{-1}) was added to the other one. Dry air was utilized as carrier gas at 10 liters per minute (lpm) for the Hafnium source and 3 lpm for the aerosol deionized water. The deposit was carried out at four different substrate temperatures: 400, 450, 500, and 550°C (the deposit time was 5 min in all cases). MOS contacts were made over the films through thermal evaporation of aluminum, achieved in a high vacuum evaporator ($10^{-5}-10^{-6}$ mbar), using a stainless-steel mask over 0.011 cm^2 with circular perforations.

2.3. Characterization of HfO_2 thin films

Thicknesses and refractive indexes of the HfO_2 films were found in an LSE Stokes Ellipsometer (Gaertner). A Magna-IR 550 FTIR (Nicolet) was employed to obtain the IR spectra in the 400-4000 cm^{-1} region, and grazing incidence X-ray diffraction (GIXRD) was performed on a Siemens D-5000 diffractometer for structural characterization. The rugosity was determined utilizing an Atomic Force Microscope (AFM) from Thermo Microscopes Veeco model auto probe CP with 10 μm scanner, and a Sirion LX30 Scan Electron Microscope (FEI) was employed to determine the morphology. A JSM-6300 (Jeol) with an EDS detector (NORAN 660B-1555) was used to get chemical composition. The C-V electrical analysis was carried out with a Keithley 5951 remote input coupler, a 590 CV analyzer, and a programmable voltage source at 100 kHz.

3. Results and discussion

3.1. Grazing incidence X-ray diffraction analysis

Figure 2a illustrates the GIXRD patterns related to a pure amorphous phase for the samples without deionized water (WoW) grown at 400°C and 450°C. The 500°C sample shows only one prominent peak with very low intensity, and the 550°C sample shows two prominent peaks located at $2\theta \sim 31.7°$ and 34.5° [28-30]. This sample exhibits better rearrangement and preferential growth. The peak (111) is the most intense in both cases; because it was parallel to the Si substrate, it grew faster than other orientations. For the samples deposited with deionized water (WW), GIXRD patterns are displayed in Fig. 2b; the added water to the mixture

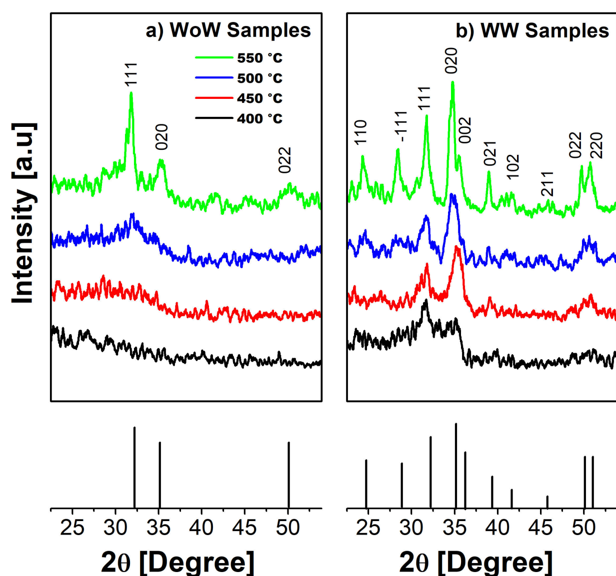

FIGURE 2. X-ray diffractograms of HfO_2 thin films grown over a Si substrate and their growth temperature dependence. a) Without Water (WoW), amorphous phase, and few small crystal formations, b) With Water (WW), the crystalline structure of the monoclinic phase of HfO_2 is very well defined.

favors crystalline structure formation in the HfO_2 thin films, independently of the growth temperature. Deionized water spray helps remove organic residue; when mixed with $Hf(acac)_4$ flow, the amount of material that reaches the surface decreases, allowing the available reaction energy to be more efficient promoting structural ordering. All the diffraction patterns correspond to the monoclinic phase of HfO_2 based on JCPDS card 34-104, with the most intensive peak centered at $2\theta \sim 34.5°$ that corresponds to the crystalline plane (020) [28-31]. This result can be expected since it is known that, at high deposition temperatures, there is higher surface energy at the substrate, which leads to adjustments and rearrangements of the atoms and/or constituent molecules of the oxide, thereby favoring the growth of crystals.

The change in the structural morphology of the WW HfO_2 thin films can be investigated by measuring the crystallite size of the (020) plane using the Scherrer equation [32]

$$D = \frac{0.9\lambda}{\beta \cos\theta}, \tag{1}$$

where D is the crystallite size, λ the X-ray wavelength (0.1541 nm), β the full width at half maximum of the peak intensity (FWHM), and θ the Bragg diffraction angle. The results are shown in Fig. 3 (black circles left side). As it is expected, there is an influence of temperature on the crystallite size; this kind of behavior has been observed and analyzed on HfO_2 thin films grown by atomic layer deposition [33]. Water steam acts as an agent that binds to the released carbon bound resulting from $Hf(acac)_4$ breakdown. Furthermore, it is a promoter of the desorption of the carbon compounds

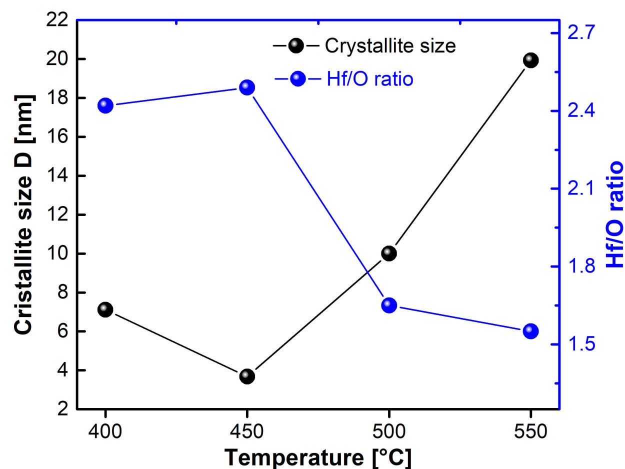

FIGURE 3. Crystallite size (black circles left side axis) and Hf/O ratio (blue circles at right-side axis) depending on the temperature calculated from the X-ray diffraction data and EDS, respectively.

from the surface. Thus, $Hf(acac)_4$ is adsorbed on the substrate, where its thermal decomposition occurs.

3.2. X-ray energy dispersive spectroscopy analysis

Figure 3 (blue circles at the right side) shows the Hf/O ratio, calculated from EDS data. For those samples deposited at 400 and 450°C, there is a more significant amount of oxygen coming from other species such as SiO_x ($x > 2$), which forms at the interface due to the thermal oxidation of the Si wafer during the deposit [34]. Additionally, the crystallite size is smaller since the thermal energy is not enough to allow the formation of larger crystals. Under these conditions, a few crystals can be formed, as observed in GIXRD. The highest Hf/O ratio was obtained for the sample deposited at 450°C. As the temperature increases, from 500 to 550°C, the thermal energy to carry the reaction increases, allowing the formation of more, better-defined crystallites and a better crystal structure, as can be appreciated from the GIXRD results (black circles at the left side). However, oxygen gradually decreases, generating vacancies, which are most common in high-k gate dielectrics and gives rise to positive charge [35].

3.3. Scanning electron microscopy analysis

Figure 4a shows a transversal view of a WW deposited sample obtained by scanning electron microscopy. It is possible to visualize the different layers forming the structure, a first region corresponding to the Si substrate, a second region showing a SiO_2 interface layer with a thickness of a few nanometers, related to the oxidation at the time of deposit (present in WoW and WW samples). A third region is related to the deposition of the HfO_2 thin film [34]. Figure 4b corresponds to the HfO_2 film surface, showing nanostructured crystals formation, in agreement with the GIXRD diffractograms and EDS measurements.

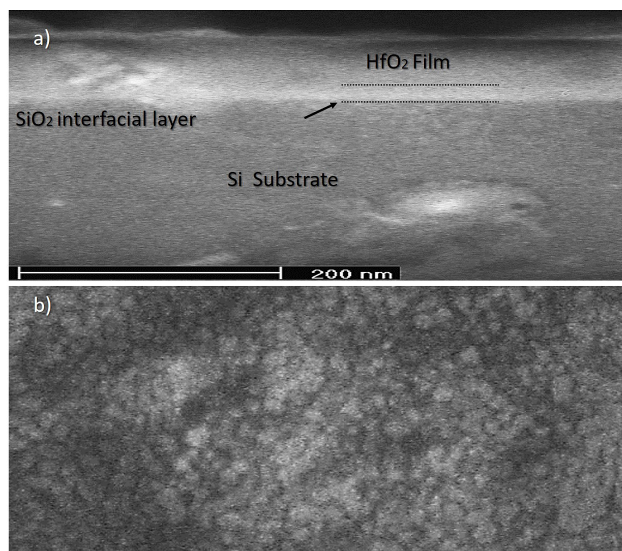

FIGURE 4. Scanning Electron Microscopy images, a) transversal view of the HfO_2 film and structure, b) top view of the HfO_2 film showing the formed nanostructures.

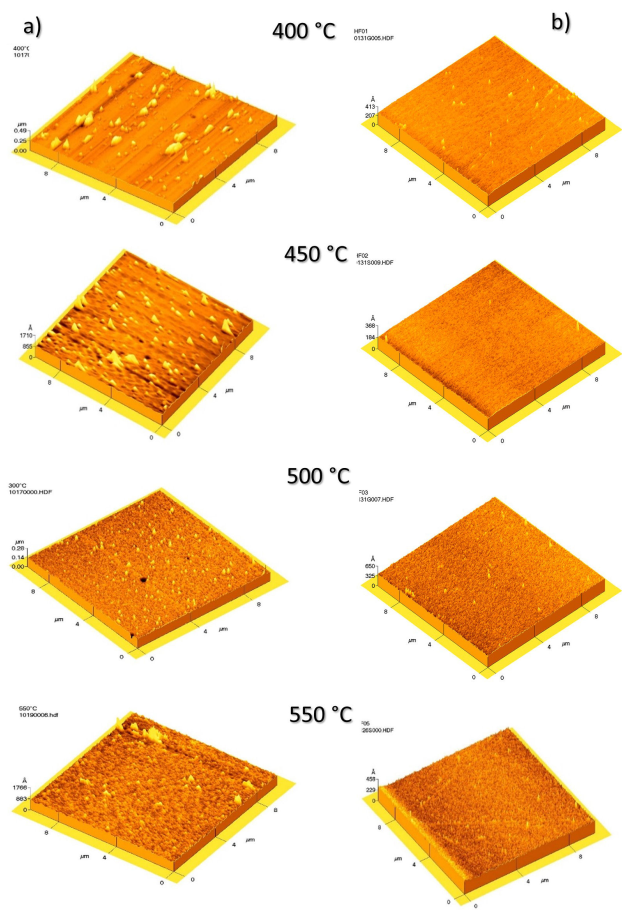

FIGURE 5. Atomic Force Microscopy shows the HfO2 thin film surface morphology, column a) WoW and column b) WW.

3.4. Atomic force microscopy

Atomic Force Microscopy shows the HfO_2 thin film surface morphology (Fig. 5). For those samples obtained without water (Fig. 5a), as substrate temperature rises, the surface rugosity decrease from 19.8 to 5.79 nm (Table I), and the film quality enhances. The Hf(acac)$_4$ thermal decomposition is more efficient, thus considerably reducing organic waste. The organic residues are more easily removed as the temperature increases. The metal part melts, forming mainly thin layers that create dense and compact films, thereby leading to low roughness surfaces.

On the other hand, the samples deposited with water under the same conditions (Fig. 5b) have a lower rugosity than the WoW. This decrease in roughness could be because water flow dilutes the solution causing a smaller amount of material to reach the substrate surface. As there is less organic waste, the metallic part melts with the substrate, forming uniform thin layers, allowing a better structural arrangement. The increase in roughness with increasing temperature for WW samples is directly related to the increase in crystallite size discussed above (Fig. 3). Another factor to consider is the irregularities caused by the SiO_x layer generated when the silicon wafer is exposed to the environment; the layer is not uniform, so the film takes the form of this interfacial layer. The film deposited at 450°C has the lowest rugosity.

3.5. Infrared (IR) spectra analysis

IR analysis for WoW samples is shown in Fig. 6a. The films deposited at 400 and 450°C present broadband centered approximately at 3400 cm^{-1} due to O-H type bonds [36,37]. This same band appears slightly on those films deposited at 500 and 550°C. The bands located at 1510 and 1410 cm^{-1}

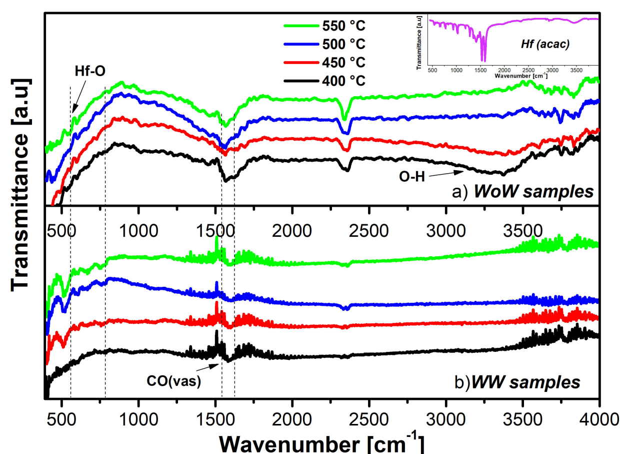

FIGURE 6. a) IR spectra from WoW samples grown from 400 to 550°C. Two bands close to 1512 and 1595 cm^{-1} related to the carbonyl groups, a band centered in 3400 cm^{-1} due to O-H bonds, are observed. b) IR spectra from WW samples. The bands related to the carbonyl groups disappear, O-H bonds noticeably decrease, and hafnium oxide bands are better defined. The Inset represents Hf(acac)$_4$ IR spectra.

correspond to vibrational modes of the asymmetric stretching of carbonyl CO(vas). It is also possible to appreciate two bands close to 1512 and 1595 cm^{-1} related to carbonyl groups. The Inset in Fig. 6 corresponds to a typical IR spectrum for $Hf(acac)_4$, showing two bands at 1530 and 1595 cm^{-1} due to carbonyl groups. Therefore, those bands observed in our samples must be associated with carbon residues because of the source reagent incomplete decomposition [38].

The bands located at 512, 635, and 752 cm^{-1} are reported for hafnium oxide with a monoclinic structure [39,40]. A small band located at approximately 750 cm^{-1} is observed in our spectra on those films deposited from 450 to 550°C. The above indicates the existence of Hf-O type bonds, consistent with the GIXRD results, where a peak corresponding to the orientation (111) of the monoclinic phase is observed for those films.

On the other hand, WW films (Fig. 6b) do not present the band centered at 3400 cm^{-1}, related to O-H type bonds. Then, if deionized water is added, there is a notable decrease in this type of bond. Additionally, the bands located around 1500 cm^{-1} appear with a lower intensity, indicating that these films are generally cleaner from carbon-associated residues [41]. Obtaining films with less carbon through water addition has already been observed in other types of films, such as aluminum oxide synthesized by LPCVD [42].

The function of deionized water steam is to promote carbon compounds desorption from the surface where the film growth occurs. WoW films at 400 and 450°C present O-H bonds, which disappear when heated, but as soon as they cool and are exposed to the environment, they physisorbed water. This does not happen with WW samples exposed to the environment [41]. The hafnium oxide bands located at 512, 635, and 752 cm^{-1}, seem to be very noticeable in almost all the spectra of Fig. 6b) [39,43]. It is observed that the band located at $\sim$ 500 cm^{-1} increases its intensity as temperature rises. For films deposited at 400°C, the band located at 500 cm^{-1} is not very noticeable in the spectrum, but those films deposited at 450, 500, and 550°C appear more intense.

3.6. Ellipsometry analysis

The thicknesses for each sample have been determined using ellipsometry (our results are presented in Table I). We have considered the average thickness evaluation in the calculations, considering the interfaces present in each of the structures as we observed from SEM (Fig. 4a). As it is observed, the thickness of WoW thin films is larger than those of WW. As we have previously mentioned, water helps to carry away those carbons left free when the salt melts, this makes the reaction slower, and a smaller amount of hafnium reaches the surface.

The refractive index was obtained employing a fixed wavelength ellipsometer. For WoW samples, the refractive index at 400 and 500°C is $n = 1.92$ (amorphous phases), and at 450 and 550°C, the values are $n = 1.96$ and $n = 2.00$, respectively, which are related to the crystallites formation with direction (002) and (111). For WW samples, the refractive index tends to increase slightly as temperature increases, consistent with the crystalline state behavior [44]. The refractive indexes acquired in this work are comparable with those obtained by Atomic Layer Deposition (ALD), with values between $n = 1.8$ and $n = 2.0$. Similar results are reported for light-assisted sol-gel synthesis, with a refractive index of $n = 1.90$ [45].

Moreover, the refractive index is related to the packing density p (dependent on the ratio of the volume of the solid part to the total volume of the film, which includes the pores), and it can be determined by the expression [46]

$$P = \frac{(n_v^2 - n^2)(n_s^2 n^2 + n_v^2 n^2)}{n^2(n_v^2 - n_s^2) + n_v^2(1 - n_s^2)}; \tag{2}$$

here n_v is the void refractive index ($n_v = 1$) and n_s is the bulk refractive index ($n_s = 2.1$). The corresponding values are reported in Table I. The packing density for the WoW samples is associated with the OH bands present in the IR analysis, induced by moisture adsorption from the thin film in the environment, presenting a variation on the refractive index (or packing density) [47,48]. On the other side, for WW samples, there is a strong correlation with GIXRD when the crystalline structure is better defined. There are slight packing density changes for samples at 400-500°C; however, the packing density increases abruptly for the 550°C sample. As the temperature increases, a better structural arrangement is generated, voids and structural defects are reduced, causing a shrinkage that affects the film thickness, and, consequently, the packing density increases [49]. Furthermore, the Hf/O

TABLE I. Rugosity, thickness, refractive index, and packing density for WoW and WW samples.

	WoW samples				WW samples			
Temperature (°C)	Rugosity (nm)	Films thickness (nm)	Refractive index	Packing density	Rugosity (nm)	Films thickness (nm)	Refractive index	Packing density
400	19.80	120.0	1.92	0.91	0.89	32.5	1.87	0.88
450	6.14	115.0	1.95	0.93	0.45	11.0	1.90	0.90
500	6.77	165.0	1.92	0.91	1.59	23.0	1.89	0.89
550	5.79	130.0	2.00	0.95	1.86	18.5	2.02	0.96

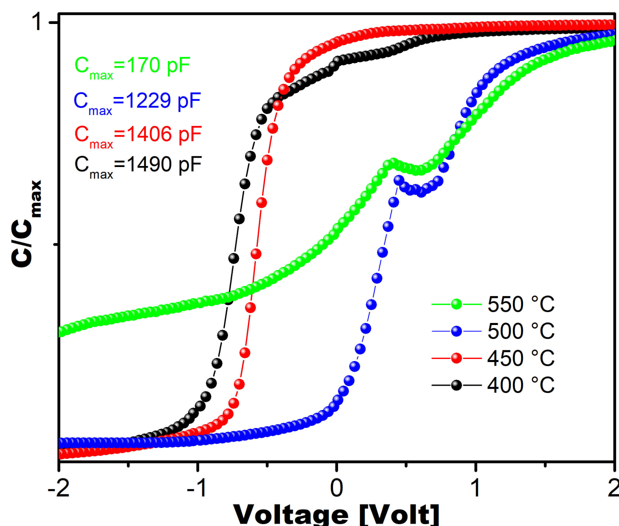

FIGURE 7. C-V normalized curves of the MOS structures made with HfO_2 WW films (WW samples) deposited at different temperatures.

ratio decreases notably for this temperature, consistent with EDS observed behavior.

3.7. C-V analysis

Figure 7 shows the C-V curves for the MOS structures made with HfO_2 films (WW samples) at different temperatures. The curves have been normalized to make a better comparison and determine the effect of temperature and water-assisted deposition on their electrical properties. The film grown at 400°C has an accumulation region at 1490 pF and a dielectric constant of 13.8; the inversion zone tends to be vertical and close to zero, presenting a slight shift to the left, related to fixed insulating loads due to a high oxygen concentration, possibly caused by the formation of the SiO_x interfacial layer [54]. There is a small hump, characteristic of slow traps present at the insulator/semiconductor interface, due to defects distributed outside the insulator interface. Therefore, the emission and capture of electrons produce a constant dispersion over time, giving rise to hysteresis in the C-V curve [55]. The graph corresponding to 450°C is the most representative of a MOS structure since the C-V curve is the best defined, with a slight shift to the left, and whose accumulation region presents a value of 1406 pF. The absence of shoulders indicates few defects and traps at the interface, showing that the C-V response is expected for an ideal dielectric material, with a dielectric constant of 14.4 [50-52]. We obtained the highest dielectric constant value and the best electrical properties for this sample than for all the synthesized samples. For samples grown at 500°C, the behavior is not typical for a MOS structure; the inversion part is slightly curved, reaching a maximum of 1229 pF and a dielectric constant of 8.5; the inversion zone has a hump. Finally, the C-V curve for the 550°C sample is the one with the least expected behavior; it is deformed, the accumulation tends to be flat over 170 pF, well below the previous samples [53]; the inversion and depletion zone is not adequately defined.

The electrical characteristics of WoW samples are not suitable for C-V calculations. This can be attributed to the SiO_2 thermal layer (up to 100 Å) between the silicon substrate and the HfO_2 film. In addition to its high thickness, the defects contribute to generating a poor electrical response. The high quality of the WW films minimizes the effect of the SiO_2 layer. This problem is still presented by films deposited by sophisticated techniques such as ALE. When HfO_2 is deposited on other materials, this problem does not arise.

4. Conclusions

We have presented the effect of deionized water-assisted synthesis of HfO_2 from Hf(acac)$_4$ by the ultrasonic pyrolytic spray technique. Our results show that vapor water favors the formation of polycrystalline films with a well-defined monoclinic phase at specific temperatures. Samples grown without the addition of deionized water are amorphous and with low structural order. The carbon and O-H bonds decrease considerably, making thinner films than those deposited without water and better controlling the HfO_2 film growth. Films deposited at 450°C have the highest dielectric constant (14.4) and do not exhibit hysteresis, in contrast to the other films; moreover, roughness has a minimum value (0.45 nm) for this sample. Therefore, the effect of deionized water during deposition on HfO_2 films improves the structural, optical, and electrical characteristics, making them compact and nanostructured.

We have shown that water-assisted ultrasonic spray pyrolysis is an excellent method to synthesize HfO_2 thin films (from metal-organic precursors) with appropriate structural optical and electrical properties for the fabrication of ultra-large-scale integration systems and technological applications such as MOSFET, CMOS, NVM, RAM card, and other devices.

Acknowledgments

The authors would like to thank M. Guerrero and Z. Rivera for their technical support.

Funding information

This work was partially supported by Sistema Nacional de Investigadores (SNI-CONACYT) & Instituto Politécnico Nacional (SIP-IPN Project Numbers 20201170 and 20201635).

1. Seok-Woo Nam *et al*, Influence of annealing condition on the properties of sputtered hafnium oxide, *Journal of Non-Crystalline Solids* **303** (2002) 139, https://doi.org/10.1016/S0022-3093(02)00976-6
2. J. Robertson, High dielectric constant gate oxides for metal oxide Si transistors, *Rep. Prog. Phys.* **69** (2006) 327, https://doi.org/10.1088/0034-4885/69/2/R02.
3. M. Balog, M. Schieber, M. Michman and S. Patai, Chemical vapor deposition and characterization of HfO_2 films from organohafnium compounds, *Thin Solid Films* **41** (1977) 247, https://doi.org/10.1016/0040-6090(77)90312-1
4. M. Villanueva-Ibañez, C. Le Luyer, O. Marty, J. Mugnier, Annealing and doping effects on the structure of europium-doped HfO_2 sol-gel material, *Optical Materials* **24** (2003) 51, https://doi.org/10.1016/S0925-3467(03)00104-6.
5. H. Padma Kumar *et al*., Optical properties of nanocrystalline HfO_2 synthesized by an auto-igniting combustion synthesis, *J. of Asian Ceramic Societies* **3** (2015), 64; https://doi.org/10.1016/j.jascer.2014.10.009
6. M. F. Al-Kuhaili, Optical properties of hafnium oxide thin films and their application in energy-efficient Windows, *Opt. Mats*. **27** (2004) 383, DOI:10.1016/j.optmat.2004.04.014
7. T. Mori, M. Fujiwara, R. R. Manory, I. Shimizu, T. Tanaka, and S. Miyake, HfO_2 thin films prepared by ion beam assisted deposition, *Surface and Coating Technology* **169** (2003) 528, https://doi.org/10.1016/S0257-8972(03)00189-0.
8. M. Alvisi, S. Scaglione, S. Martelli, A. Rizzo, and L. Vasanelli, Structural and optical modification in hafnium oxide thin films related to the momentum parameter transferred by ion beam assistance, *Thin Solid Films* **354** (1999) 19, https://doi.org/10.1016/S0040-6090(99)00534-9.
9. H. Ibégazéne, S. Alpérine, and C. Diot, Yttria-stabilized hafnia-zirconia thermal barrier coatings: The influence of hafnia addition on TBC structure and high-temperature behaviour, *J. Mater. Sci.* **30** (1995) 938, https://doi.org/10.1007/BF01178428.
10. J. Wang, H.P. Li, R. Stevens, Hafnia and hafnia-toughened ceramics, *J. Mater. Sci*. **27** (1992) 5397, https://doi.org/10.1007/BF00541601.
11. V. Dave, P. K. Mishra, and R. Chandra, Nanostructured Hafnium Oxide Thin films for Sensing Carbon Monoxide: An Experimental Investigation, *Materials Today: Proceedings* **5** (2018) 23286, https://doi.org/10.1016/j.matpr.2018.11.062.
12. J.C. Guzmán Olguin *et al.*, Tunable white light emission from hafnium oxide films co-doped with trivalent terbium and europium ions deposited by Pyrosol technique, *Phys. Status Solidi A* **214** (2017) 1700269, https://doi.org/10.1002/pssa.201700269.
13. M. Aguilar-Frutis *et al*., Aluminum oxide thin films deposited on silicon substrates from Al(NO3)3 and an organic solvent by spray pyrolysis, *Phys Stat Sol* **199** (2003) 227, https://doi.org/10.1002/pssa.200306642.
14. P. Murugavel, M. Kalaiselvam, A. R. Raju and C. N. R. Rao, Sub-micrometre spherical particles of TiO2, ZrO2 and PZT by nebulized spray pyrolysis of metal-organic precursors, *J. Mater. Chem*. **7** (1997) 1433, https://doi.org/10.1039/A700301C.
15. S.J. Wang *et al*., Reaction of SiO2 with hafnium oxide in low oxygen pressure, *Applied Physics Letters* **82** (2003) 2047, https://doi.org/10.1063/1.1565182.
16. M. J. Biercuk, D. J. Monsma, M. Marcus, J. S. Becker, and R. G. Gordon, Low-temperature atomic-layer-deposition lift-off method for microelectronic and nanoelectronic applications, *Applied Physics Letters* **83** (2003) 2405, https://doi.org/10.1063/1.1612904.
17. M. Y. Ho *et al*., Morphology and crystallization kinetics in HfO_2 thin films grown by atomic layer deposition, *Journal of Applied Physics* **93** (2003)1477, https://doi.org/10.1063/1.1534381.
18. R. Chow, S. Falabella, G. E. Loomis, F. Rainer, C. J. Stolz and M. R. Kozlowski, Reactive evaporation of low-defect density hafnia, *Applied Optics* **32** (1993) 5567, https://doi.org/10.1364/AO.32.005567
19. P. S. Lysaght, B. Foran, G. Bersuker, P. J. Chen, R. W. Murto and H. R. Huff, Physicochemical properties of HfO_2 in response to rapid thermal anneal, *Applied Physics Letters* **82** (2003) 1266, https://doi.org/10.1063/1.1553998.
20. M. F. Al-Kuhaili, S. M. A. Durrani and E. E. Khawaja, Characterization of hafnium oxide thin films prepared by electron beam evaporation, *Journal of Physics D: Applied Physics* **37** (2004) 1254, https://doi.org/10.1088/0022-3727/37/8/015.
21. J. P. Lehan, Y. Mao, B. G. Bovard and H. A. Macleod, Optical and microstructural properties of hafnium dioxide thin films, *Thin Solid Films* **203** (1991) 227, https://doi.org/10.1016/0040-6090(91)90131-G.
22. M. Gilo and N. Croitoru, Study of HfO_2 films prepared by ion- assisted deposition using a gridless end-hall ion source, *Thin Solid Films* **350** (1999) 203, https://doi.org/10.1016/S0040-6090(99)00226-6.
23. P. Baumeister and O. Arnon, Use of hafnium dioxide in multilayer dielectric reflectors for the near uv, *Applied Optics* **16** (1977) 439, https://doi.org/10.1364/AO.16.000439.
24. M. Villanueva-Ibañez, C. Le Luyer, C. Dujardin and J. Mugnier, Elaboration, strucutural and spectroscopic properties of rare earth-doped yttrium-hafnium sol-gel oxide powders for scintillation applications, *Materials Science and Engineering B* **105** (2003) 12, https://doi.org/10.1016/j.mseb.2003.08.006.
25. M. Langlet and J. C. Joubert, *Chemistry of Advanced Materials*, in: C.N.R. Rao (Ed.) (Blackwell Science, Oxford, England, ISBN 063203385,1 (1993)) p. 55.
26. T.T. Koda and M.J. Hampden-Smith, *Aerosol processing of Materials*, (Wiley-VCH, New York, 1999), p. 537.
27. H. Huff and D. Gilmer, *Hig K gate Dielectrics* (Berlin: Springer, (ed) 2004).

28. J. Aarik, A. Aidla, and A. A. Kiisler, Influence of substrate temperature and atomic layer growth and properties of HfO_2 thin films, *Thin Solid Films* **340** (1999) 110, https://doi.org/10.1016/S0040-6090(98)01356-X.
29. D. H. Triyoso, R. I. Hegde, Bruce E. White, Jr. and Philip J. Tobin., Physical and electrical characteristics of atomic-layer-deposited hafnium dioxide formed using hafnium tetrachloride and tetrakis (ethylmethylaminohafnium), *J. Appl. Phys.* **97** (2005) 124107, https://doi.org/10.1063/1.1947389.
30. K. Kukli, M. Ritala, M. Leskelä, and T. Sajavaara, Comparision of hafnium oxide films grown by atomic layer deposition from iodide and chloride precursors, *Thin Solid Films* **416** (2002) 72, https://doi.org/10.1016/S0040-6090(02)00612-0
31. S. Tongpeng *et al*., Fabrication characterization of hafnium oxide thin films, *Materials Today: Proceedings* **17** (2019) 1555, https://doi.org/10.1016/j.matpr.2019.06.181.
32. A.L. Patterson, The Scherrer Formula for X-Ray Particle Size Determination, *Phys. Rev.* **56** (1939) 978, https://doi.org/10.1103/PhysRev.56.978.
33. J. Aarik, A. Aidla, H. Mändar, V. Sammelselg and T. Uustare, Texture development in nanocrystalline hafnium dioxide thin films grown by atomic layer deposition, *Journal of Crystal Growth* **220** (2000) 105, https://doi.org/10.1016/S0022-0248(00)00831-9.
34. M. Cho, J. Park, H. Bae Park, and C. Seong Hwang, Chemical interaction between atomic-layer-deposited HfO_2 thin films and the Si substrate, *Appl. Phys. Lett.* **81** (2002) 334, https://doi.org/10.1063/1.1492320.
35. A. S. Foster, F. Lopez Gejo, A. L. Shluger, and R. M. Nieminen, Vacancy and interstitial defects in hafnia, *Phys. Rev. B* **65** (2002) 174117, https://doi.org/10.1103/PhysRevB.65.174117.
36. J. J. Yu, Q. Fang, J. -Y. Zhang, Z. M. Wang, and I. W. Boyd, Hafnium oxide layers derived by photo-assited sol-gel processing, *Applied Surface Science* **208** (2003) 676, https://doi.org/10.1016/S0169-4332(02)01424-1.
37. J. F. Damlencourt, O. Renault, D. Samor, Electrical and physico-chemical characterization of HfO_2/SiO2 gate oxide stacks prepared by atomic layer deposition, *Solid-State Electronics* **47** (2003) 1613, https://doi.org/10.1016/S0038-1101(03)00170-9.
38. H. Guo, W. Zhang, L. Lou, A. Brioude and J. Mugnier, Structure and optical properties of rare earth doped Y2O3 waveguide films derived by sol-gel process, *Thin Solid Films* **458** (2004) 274, https://doi.org/10.1016/j.tsf.2003.12.059.
39. A. Deshpande, R. Inman, G. Jursich and C. G. Takoudis, Annealing behavior of atomic layer deposited hafnium oxide on silicon: Changes at the interface, *J. Appl. Phys*. **99** (2006) 094102, https://doi.org/10.1063/1.2191434.
40. X. Wang and L. Andrews, Infrared spectrum and structure of the Hf(OH)4 molecule, *Inorg. Chem*. **44** (2005) 7189, https://doi.org/10.1021/ic050614a.
41. M. M. Frank, S. Sayan, S. Dörman, T. J. Emge, Hafnium oxide gate dielectrics grown from an alkoxide precursor: structure and defects, *Materials Science and Engineering: B* **109** (2004) 6, https://doi.org/10.1016/j.mseb.2003.10.020.
42. J. S. Kim, H. A. Marzouk, P. J. Reucroft, J. D. Robertson, C. E. Hamrín, Fabrication of aluminum oxide thin films by a low-pressure metal-organic chemical vapor deposition technique, *Appl. Phys. Lett*. **62** (1993) 681, https://doi.org/10.1063/1.108838.
43. D. A. Neumayer, E. Cartier, Materials characterization of ZrO_2-SiO_2 and HfO_2-SiO_2 binary oxides deposited by chemical solution deposition, *Journal of Applied Physics* **90** (2001) 1801, https://doi.org/10.1063/1.1382851.
44. M. Modreanu, J. Sancho-Parramon, D. O'Cornell, J. Justice, O. Durand and B. Servet, Solid phase crystallisation of HfO_2 thin films, *Materials Science and Engineering: B* **118** (2005) 127, https://doi.org/10.1016/j.mseb.2004.12.068.
45. K. Kukli, M. Ritala, M. Leskelä, and T. Sajavaara, Atomic Layer Deposition of Hafnium Dioxide Films from 1-Methoxy-2-methyl-2-propanolate Complex of Hafnium, *Chem. Mater* **15** (2003) 1722, https://doi.org/10.1021/cm021328p.
46. J.-Chan Park, Y.-Sup Yoon, and S.-Jun Kang, Structural and Optical Properties of HfO_2 Films on Sapphire Annealed in O2 Ambient, *Journal of the Korean Ceramic Society* **53** (2016) 563, https://doi.org/10.4191/kcers.2016.53.5.563.
47. M. J. Esplendiu, E. M. Patrito and V. A. Macagno, Ellipsometric investigation of anodic hafnium oxide films, *Electrochimica Acta* **42** (1997) 1315, https://doi.org/10.1016/S0013-4686(96)00256-3.
48. W. Liu, Z. Liu, Feng Yan, T. Tan and H. Tian, Influence of O2/Ar flow ratio on the structure and optical properties of sputtered hafnium dioxide thin films, *Surface and Coatings Technology* **205** (2010) 2120, https://doi.org/10.1016/j.surfcoat.2010.08.116.
49. S. Bashir Khan, Z. Zhang and S. Long Lee, Annealing influence on optical performance of HfO_2 thin films, *Journal of Alloys and Compounds* **816** (2020) 152552, https://doi.org/10.1016/j.jallcom.2019.152552.
50. K. Takahashi, M. Nakayama, and S. Yokohama, Preparation of hafnium oxide films from oxygen-free Hf $[N(C_2H_5)_2]_4$ precursor and their properties, *Applied Surface Science* **216** (2003) 296, https://doi.org/10.1016/S0169-4332(03)00435-5.
51. Dina H. Triyoso, Impact of titanium addition on film characteristics of HfO_2 gate dielectrics deposited by atomic layer deposition, *Journal of Applied Physics* **98** (2005) 054104, https://doi.org/10.1063/1.2030407.
52. C. M. Lopez and E. A. Irene, A study of HfO_2 film interfaces with Si and SiO2, *Journal of Applied Physics* **99** (2006) 024101, https://doi.org/10.1063/1.2161411.
53. J. Arik, J. Sundqvist, A. Aidla, J. Lu, Timo Sajavaara, Hafnium tetraiodide and oxygen as precursors for atomic layer deposition of hafnium oxide thin films, *Thin Solid Films* **418** (2002) 69, https://doi.org/10.1016/S0040-6090(02)00765-4.

54. L. Khomenkova, B. S Sahu, A. Slaoui and F. Gourbilleau, Hf-based high-k materials for Si nanocrystal floating gate memories, *Nanoscale Research Letters* **6** (2011) 172, https://doi.org/10.1186/1556-276X-6-172.

55. A. Callegari, E. Cartier, M. Gribelyuk, H. F. Okorn-Schmidt and T. Zabel, Physical and electrical characterization of Hafnium oxide and Hafnium silicate sputtered films, *Journal of Applied Physics* **90** (2001) 6466, https://aip.scitation.org/doi/10.1063/1.1417991.